Int. J. Heat Mass Transfer. Vol. 29, No. 8, pp. 1185–1191, 1986
Printed in Great Britain

0017-9310/86 $3.00 + 0.00
Pergamon Journals Ltd.

Effect of angle of attack on the heat transfer coefficient for an annular fin

E. M. SPARROW and S. R. CHASTAIN

Department of Mechanical Engineering, University of Minnesota, Minneapolis, MN 55455, U.S.A.

Abstract—Wind-tunnel experiments were performed to investigate the sensitivity of the heat transfer coefficient for an annular fin to small angles of attack. Quasi-local measurements were made at three zones on the fin surface: (I) forward of the tube; (II) at the side of the tube; and (III) behind the tube, with separate measurements being carried out on the two faces of the fin. The angle of attack ranged from $-2°$ to $2°$. The heat transfer coefficient in zone (I) was highly sensitive to the angle of attack, increasing by about 50% on the face of the fin where leading-edge separation was activated as the angle was varied from $-2°$ to $2°$. The corresponding increases in zones (II) and (III) were about 10%. On the other hand, for any angle of attack in the investigated range, the two-face average for each zone was not very different from the heat transfer coefficient for zero angle of attack. Therefore, the overall heat transfer performance of an annular fin is not significantly affected by small departures of the angle of attack from zero. However, since the differences between the coefficients for the two faces were found to be significant, measurement of the coefficient at only one face may yield erroneous results for the overall performance.

1. INTRODUCTION

AN ANNULAR finned tube situated in a forced convection crossflow creates and is washed by a highly complex flow field. The key features of the flow include separation at the leading edge of the fin, vortices formed by the interaction between the boundary layers on the fin surfaces and the tubes, and the separated region at the rear of the tubes. The effects of these processes on the heat transfer characteristics of annular-finned tubes have not been investigated. From experiments on flat plates with blunt leading edges, leading-edge separation was found to enhance heat transfer [1, 2]. Experimental work on a strip-finned crossflow tube bank showed the vortices to be enhancing, while the tube rear-face separation reduced the heat transfer [3].

Since some or all of these fluid flow processes may be sensitive to the angle of attack at which the free-stream arrives at the finned tube, so, too, may the heat transfer respond strongly to changes in the angle of attack. The focus of the present work is to experimentally investigate the response of the heat transfer and fluid flow at an annular finned tube to variations of the angle of attack.

As a logical first step in the research, consideration was given to the limiting case of a tube equipped with a single annular fin. The results for this case can serve as a baseline against which the results for multifin arrays can be compared. In addition, for small angles of attack, which constitute the range most relevant to practice, the single fin results should approximate those for an intermediate- or large-pitch multifin array.

Preliminary experiments showed the most significant effects of a non-zero angle of attack occurred at small angles of attack. Consequently, the experimental work was concentrated on angles of attack in the range from $-2°$ to $2°$. The heat transfer response to the variation of the angle of attack was measured by a mass transfer sensor, which was a thin film of naphthalene that had been cast into a recess in the surface of the fin. At each angle of attack, individual data runs were made with the sensor positioned at different circumferential locations on the annular fin. In addition, in companion data runs, the sensor was alternately positioned on the windward face of the fin and on the leeward face, both at a common circumferential location. The fluid flow response to variations of the angle of attack was visualized by use of the oil–lampblack technique, which provided a record of the pattern of fluid flow adjacent to the surface of the fin.

2. EXPERIMENTS

The description of the experimental apparatus is facilitated by reference to Fig. 1. The (a) part of the figure is a schematic side view showing the annular fin in place in the host tube, while the (b) part is a full-face view of the fin.

The fin was fabricated from brass, with a diameter of 7.696 cm and a finished thickness of 0.124 cm. Special care was taken to ensure the flatness of the fin, and its faces were hand lapped to a high degree of smoothness. The fin tip was beveled at an angle of 45° to help avoid blunt-edge effects. A 0.963-cm center hole was provided to accommodate a shaft which facilitated the assembly of the apparatus.

The fin was recessed to accommodate a thin layer of naphthalene, which is designated by black shading in the figure. As seen in Fig. 1 (b), the recess is a 30° annular sector whose inner and outer diameters are 2.540 and 7.696 cm, respectively, with a depth of

NOMENCLATURE

A	mass transfer surface area
D_f	outer diameter of fin
D_t	diameter of tube
$\mathscr{D}$	mass diffusion coefficient
K	mass transfer coefficient
ΔM	mass sublimed during data run
Re_f	Reynolds number, $U_\infty D_f/\nu$
Re_t	Reynolds number, $U_\infty D_t/\nu$
Sc	Schmidt number
Sh	Sherwood number
U_∞	freestream velocity.

Greek symbols

α	angle of attack, Fig. 1 (a)
θ	circumferential position of mass transfer zone, Fig. 1 (b)
ν	kinematic viscosity
ρ_{nw}	naphthalene vapor density at subliming surface
$\rho_{n\infty}$	naphthalene vapor density in freestream
τ	duration of data run.

0.56 cm. The surface area of the exposed naphthalene was chosen so that for a 0.0025-cm recession of the surface due to sublimation, the sublimed mass was approximately 0.01 g. The limitation of the recession to 0.0025 cm was imposed to avoid significant alteration of the fin surface configuration, while the measurement of a 0.01-g change of mass was the smallest value compatible with the available instrumentation.

The naphthalene layer was created by a casting procedure, for which the fin itself was one part of the mold. The other parts transformed the recess into a mold cavity, into which molten naphthalene was poured through small holes which penetrated the bottom of the recess from behind. Those mold parts which contacted the naphthalene surface subsequently to be exposed to the air flow were lapped to a mirror finish. The mold was contoured so that the cast naphthalene continued the beveled edge of the remainder of the fin. The beveled edge of the naphthalene was coated by a very thin impermeable film (white glue) to prevent sublimation there.

Subsequent to the casting, the pour holes were sealed with 0.002-cm-thick, pressure-sensitive tape. To prevent sublimation of the naphthalene surface at times other than during a data run, a tight-fitting nylon cover was used to cap the surface.

The fin was supported between the faces of sections of thick-walled tube as shown in Fig. 1 (a). The tube sections were fabricated from aluminum rod stock, with finished outer and bore diameters of 2.54 and 0.963 cm. A 0.953-cm diameter brass rod passed through the tube bore and the center hole of the fin. It was threaded at both ends to enable force to be applied for the attainment of a rigid structure.

For the experiments, the fin-tube assembly was situated in a low-speed, low-turbulence (0.4% turbulence level) wind tunnel. The test section of the tunnel had a 30.48×60.96 cm (height $\times$ width) cross section and was 244 cm in length. The tube was positioned vertically in the cross section, midway between the side walls.

The tunnel was operated in the open-circuit mode and in suction, with air drawn from the interior of the building and discharged outside. The freestream velocity was measured by an impact tube in conjunction with a wall static tap, both situated just

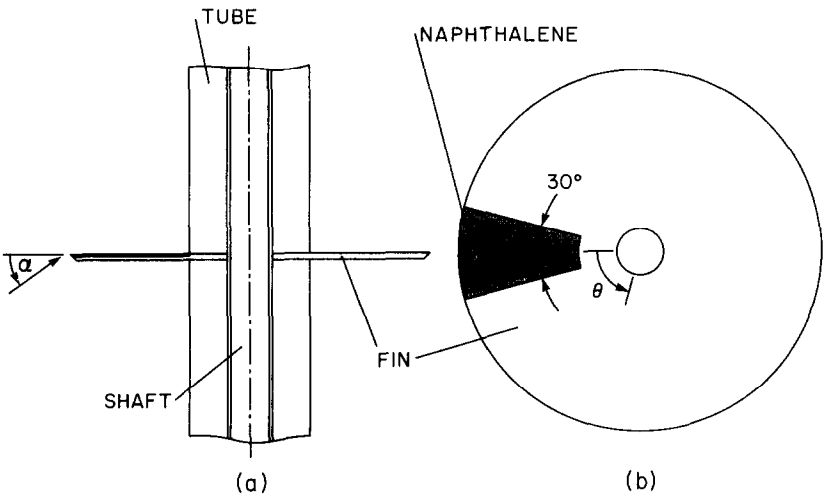

FIG. 1. Schematic diagrams of the fin–tube assembly and of the fin.

upstream and to the side of the finned tube. The pressure signals were read by a solid-state, capacitance-type pressure meter with a resolution of 0.001 Torr. With regard to temperature, auxiliary experiments had demonstrated that the readings of a thermocouple embedded in the naphthalene film and of a thermometer exposed to the airflow agreed to about 0.1°F. Owing to practical difficulties involved with embedding a thermocouple in so thin a film, the thermometer (ASTM-certified, smallest scale division = 0.1°F) was used for the final data runs.

The primary parameter that was varied during the course of the experiments is the angle of attack α, which is illustrated in Fig. 1(a). The angle of attack was set relative to the floor of the wind tunnel under the assumption that the freestream velocity was parallel to the floor (to be verified later). A non-zero angle of attack was created by inclining the fin–tube assembly relative to the freestream flow. The inclination was accomplished by placing small pieces of shim material between the bottom face of the tube and the floor.

The setting of the angle of attack is believed to be accurate to 0.05°. It was carried out in three steps. First, a sine bar placed on the floor of the wind tunnel was inclined at the desired angle α by means of gage blocks inserted between the supports of the sine bar and the floor. Then, an adjustable protractor head was placed atop the sine bar, and the bubble in the bubble level attached to the protractor head was brought to a reference mark. Finally, the protractor head was placed on the fin, and pieces of shim material were introduced at the base of the tube until the bubble was, once again, at the reference mark.

The other parameter of the experiments was the circumferential location of the mass transfer zone. As indicated in Fig. 1(b), the polar coordinate θ was used to specify the circumferential location (note that the radial line which specifies the angle θ bisects the 30° arc spanned by the mass transfer zone). The circumferential location was set by matching reference lines drawn on the floor of the wind tunnel with corresponding lines on the fin. During the course of the experiments, the mass transfer zone was situated at either $\theta = 0$, 90 or 180°.

Each data run was initiated by the weighing of the fin, after which the mass transfer zone was capped to prevent sublimation. Then, the fin–tube assembly was set up and installed in the wind tunnel. The airflow was then activated and a half-hour period was allowed for the fin to attain thermal equilibrium with the flow. During the equilibration period, the mass transfer zone was kept tighly capped and, as an additional defense against sublimation, a plastic wrap was applied.

The data run proper was initiated with the removal of the cap and the wrap. The duration of the run was chosen to obtain a sublimation mass transfer of about 0.01 g (for reasons discussed earlier). During the run, periodic readings were taken of the velocity pressure, air temperature, tunnel static pressure and barometric pressure. The run was terminated with the capping of the mass transfer zone and disassembly of the apparatus, after which the fin was weighed (with the cap removed). The weighing was performed using an electronic analytical balance with a resolution of 0.00001 g.

Supplementary experiments were carried out to assess the extent of any extraneous mass transfer which might have occurred between the initial and final weighings of the fin. From these experiments, a correction of about 1% was determined.

All of the experiments were performed at a freestream velocity of about 12 m s^{-1}, which corresponds to a tube-diameter Reynolds number of 18,800 and a fin-diameter Reynolds number of 56,500.

3. FLOW VISUALIZATION

The oil–lampblack technique [4, pp. 53–56] was employed to visualize the pattern of fluid flow adjacent to the fin surface, revealing such phenomena as separation, recirculation and reattachment. This technique was implemented by first preparing a suitably fluid mixture of lampblack powder and oil. The mixture was applied uniformly to the upfacing surface of the fin, yielding a glossy black coating. When the coated fin was subjected to the airflow, the oil–lampblack mixture was rearranged by the shear and pressure forces to form an image of the surface-adjacent flow pattern. In regions of low velocity, the mixture remained stationary, giving rise to black zones in the visualization pattern. After the airflow period, the fin was removed from the wind tunnel and the visualization pattern was photographed.

To provide a contrasting background for the visualization pattern, white, plasticized, self-adhering contact paper was affixed to the surface of the fin prior to the application of the oil–lampblack mixture. The upfacing surface of the fin was chosen for the visualization work rather than the downfacing surface because the mixture, when applied to the latter, would have tended to drip and/or sag under gravity.

As an alternative to the aforementioned uniform application of the oil–lampblack mixture, small discrete drops were placed on the surface. Observations of the motion of the droplets in the presence of the airflow were made and recorded.

Representative flow visualization results are presented in Figs. 2 and 3. The first of these figures is for positive angles of attack (i.e. 1° or 2°), while the second is for negative angles of attack (−1° or −2°). Each figure contains two diagrams, the oil–lampblack visualization pattern at the left and an interpretation of the visualization pattern at the right. The decisive difference between the results of Figs. 2 and 3 is the presence, for the former, of flow separation on the forward portion of the fin while, for the latter, the separation is absent.

Attention will first be focused on Fig. 2. The

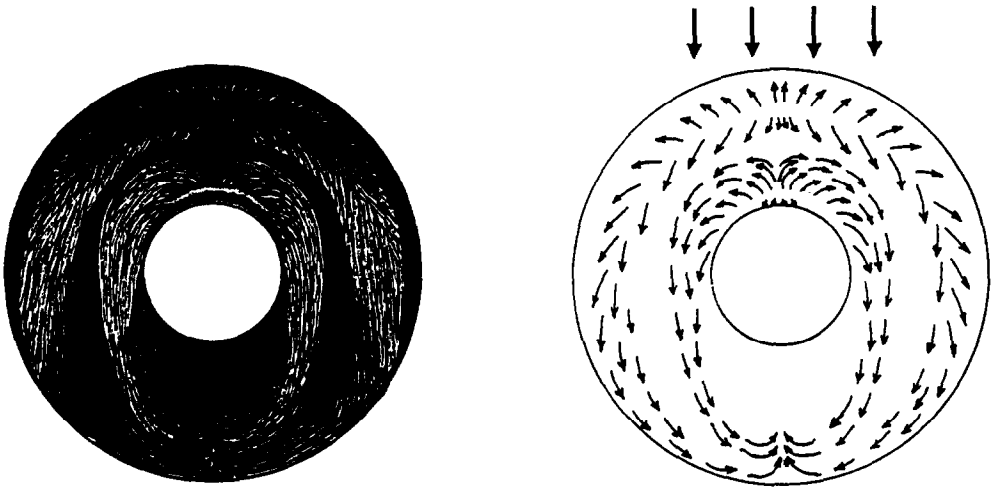

FIG. 2. Flow visualization results in the presence of forward-edge separation.

discussion of the figure will start from the forward edge of the fin and proceed downstream. From the interpretative diagram, it is seen that there is a zone of backflow (i.e. flow with a velocity component opposite to the freestream direction) adjacent to the forward edge. The backflow is the surface-adjacent leg of a recirculation zone which results from the separation of the flow at the edge. The reattachment of the separated flow is represented by a black band just downstream of the aforementioned zone of backflow.

A boundary layer begins to develop downstream of the reattachment, as represented by the forward-directed vectors. The boundary-layer flow must, however, move against an adverse pressure gradient which results from the stagnation that occurs at the forward part of the tube. The presence of the adverse pressure gradient causes the boundary layer to separate, as indicated by the black band situated downstream of the boundary-layer region.

The region directly in front of the tube contains a system of vortices. Their imprint on the fin surface is a relatively broad backflow region followed by a low-velocity intervortex zone (a narrow black band) and then by a narrow region of forward flow (the thin white arc immediately adjacent to the tube surface). The axes about which the vortices rotate are perpendicular to the symmetry plane of the flow pattern. Swirling air is discharged from the sides of these vortices and is swept around each side of the tube, forming an inverted U which is wrapped around the tube. The U-shaped portion of the vortex system is often referred to in the literature as a horseshoe vortex.

The aforementioned horseshoe vortex might well be termed the *inner* horseshoe vortex, since there exists another horseshoe vortex which is situated closer to the rim of the fin. The outer horseshoe vortex is formed by the deflected boundary-layer flow and by the deflected flow from the forward, edge-adjacent recirculation zone. Between the two horseshoe vortices,

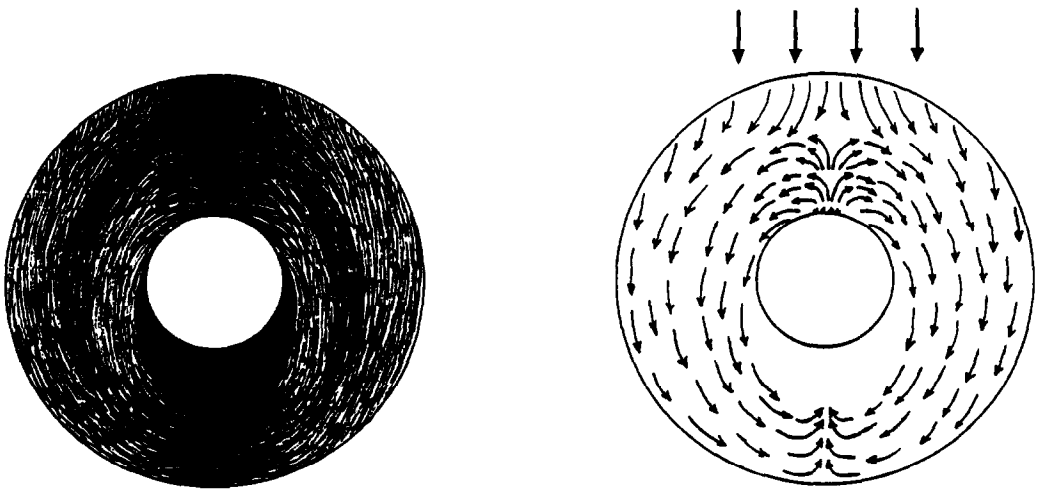

FIG. 3. Flow visualization results in the absence of forward-edge separation.

there is a region of slow-moving fluid (i.e. a black region) which is a continuation of the boundary layer separation zone.

The region directly downstream of the tube also appears black in the visualization diagram. This is a separated region—the wake of the tube. The separation occurs at about $\theta = 90°$.

Attention will now be turned to Fig. 3. Here, there is no forward-edge separation and, correspondingly, the recirculation and reattachment zones of Fig. 2 are absent. Rather, boundary-layer development is initiated at the edge. As before, the boundary layer separates owing to the adverse pressure gradient and is deflected around the sides of the tube. The vortex system situated in front of the tube appears to extend farther upstream than before. It also appears that there are now two distinct vortices having backflow traces on the fin surface rather than one, in addition to the compact forward-flow vortex immediately adjacent to the tube.

The demarcation between the inner and outer horseshoe vortices is now less distinct. Furthermore, it appears that the flow closes up sooner around the wake behind the tube.

The foregoing discussion has called attention to the significant differences in the flow patterns corresponding to the presence or absence of forward-edge separation. It is noteworthy that these different flow patterns can be activated by remarkably small changes ($\sim 0.5°$) in the angle of attack. It is not unreasonable to expect comparable sensitivity in the heat or mass transfer.

4. MASS TRANSFER RESULTS

The mass transfer results will be reported in dimensionless terms via the Sherwood number, the mass transfer analog of the Nusselt number, which is defined as

$$Sh = KD_f/\mathscr{D} \tag{1}$$

in which K is the mass transfer coefficient, D_f is the outer diameter of the annular fin and $\mathscr{D}$ is the mass diffusion coefficient. In turn, the mass transfer coefficient was evaluated from the experimental data by using the defining equation

$$K = (\Delta M/\tau A)/(\rho_{nw} - \rho_{n\infty}). \tag{2}$$

In equation (2), the quantity ΔM is the mass sublimed during the duration τ of a data run and A is the area of the mass transfer surface. In the denominator, ρ_{nw} and $\rho_{n\infty}$ respectively denote the densities of naphthalene vapor at the subliming surface and in the freestream. The latter was zero in the present experiments. For the former, the vapor pressure–temperature relation for solid–vapor equilibrium of naphthalene [5] was used in conjunction with the perfect gas law, with the measured temperature as input.

The naphthalene–air mass diffusion coefficient $\mathscr{D}$ appearing in equation (1) was evaluated from a formula given by Skelland [6, pp. 49–51]. The diffusion coefficient was also used to evaluate the Schmidt number $Sc = \nu/\mathscr{D}$ which is the mass transfer analog of the Prandtl number, yielding a value of 2.55.

The Reynolds number may be defined either as $Re_f = U_\infty D_f/\nu$ or $Re_t = U_\infty D_t/\nu$, depending on whether the fin outer diameter D_f or the tube diameter D_t is used as the characteristic dimension. As noted earlier, the experiments were performed for $Re_t = 18{,}800$, which corresponds to $Re_f = 56{,}500$.

The Sherwood numbers measured with the mass transfer zone at $\theta = 0°$ (i.e. forward of the tube) are presented in Fig. 4 as a function of the angle of attack α, which extends from $-2°$ to $2°$. The figure contains two sets of data. In one, the data were collected with the mass transfer zone facing upward, as is illustrated in Fig. 1(a). In the other, the mass transfer zone faced downward. Curves have been faired through the data for continuity.

From the figure, it is seen that at the top face of the fin, the Sherwood number increases by about 50% as α varies from $-2°$ to $2°$. A similar increase occurs at the bottom face for α variations between $2°$ and $-2°$. The Sh vs α distributions for the top and bottom faces of the fin are virtually mirror images of each other, as they should be under ideal conditions. The two distributions intersect at $\alpha = -0.3°$, indicating a $0.3°$ offset between the freestream velocity vector and the wind tunnel floor. In view of the similarity of the results for the two faces, it is only necessary to consider one of the faces, e.g. the top face.

The flat portion of the distribution, which prevails between $\alpha = -2°$ and $-1°$, corresponds to flow without separation at the forward edge of the fin. Thereafter, as α is increased and separation is triggered, Sh rises in a step-like manner. With further increases in α, Sh continues to rise but at a slower rate.

The just-discussed great increase of the Sherwood number with the angle of attack is believed to be due

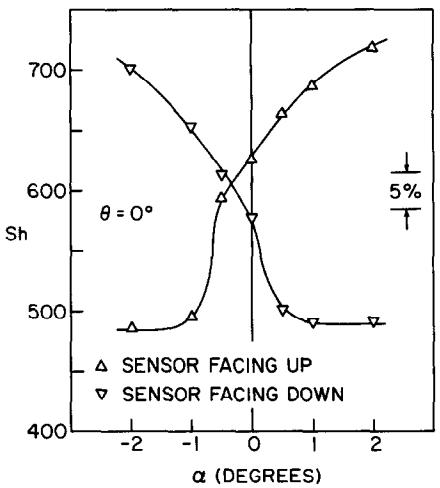

FIG. 4. Sherwood number response to angle of attack; mass transfer sensor at $\theta = 0°$.

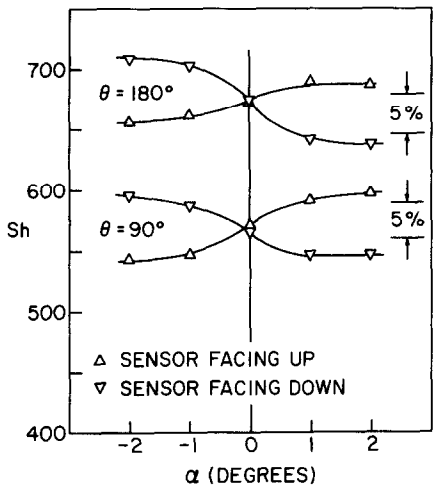

FIG. 5. Sherwood number response to angle of attack; mass transfer sensor at $\theta = 90°$ and 180°.

primarily to the separation–reattachment–redevelopment process which occurs at the forward part of the fin. According to the flow visualization results, there appear to be some differences in the vortex system situated in front of the tube depending on the presence or the absence of forward-edge separation, but the effect of these differences could not be evaluated with the type of sensor employed here.

The Sherwood number results for $\theta = 90°$ and 180° are presented in Fig. 5. At $\theta = 90°$, the mass transfer zone is at the side of the tube, while for $\theta = 180°$, it is directly downstream of the tube.

At both of these locations, the overall trend of *Sh* increasing with α at the top face of the fin and decreasing with α at the bottom face of the fin continues in force. However, the sensitivity of *Sh* to α is dramatically reduced compared to that in evidence in Fig. 4 (i.e. a 10% effect instead of a 50% effect). Thus, it appears that away from the region where the forward-edge separation process has a direct role in the mass (heat) transfer process, the mass (heat) transfer is only moderately affected by the separation.

An unexpected result seen in Fig. 5 is that the Sherwood numbers at the $\theta = 180°$ mass transfer zone are higher than those at the $\theta = 90°$ zone. It is conjectured that the high Sherwood numbers at $\theta = 180°$ are the result of vortex shedding from the tube and its interaction with the inner horseshoe vortex, which curves inward at the trailing edge.

5. CONCLUDING REMARKS

In considering the results of Figs. 4 and 5, it is relevant to note that the overall performance of a fin represents an average of the heat transfer rates at both faces of the fin. With this in mind, the *Sh* distributions of Fig. 4 for the top and bottom faces of the fin were averaged at each α value. The averages were found to deviate by no more than 6% from the *Sh* value at the intersection of the two distributions. The averages for the $\theta = 90°$ and 180° distributions agree even more closely with the respective values at the crossings of the distribution curves.

From the foregoing, it may be concluded that the overall heat transfer performance of an annular fin is not significantly affected by small departures from the case of zero angle of attack. However, since the differences between the heat transfer coefficients for the two faces of the fin were found to be significant, measurement of the coefficient at only one face may yield erroneous results for the overall heat transfer performance.

REFERENCES

1. T. Ota and N. Kon, Heat transfer in the separated and reattached flow on a blunt flat plate, *J. Heat Transfer* **96,** 459–462 (1974).
2. V. Kottke, H. Blenke and K. G. Schmidt, The influence of nose section and turbulence intensity on the flow around thick plates in parallel flow, *Wärme- u. Stoffübertr.* **10,** 159–174 (1977).
3. F. E. M. Saboya and E. M. Sparrow, Local and average transfer coefficients for one-row plate fin and tube heat exchanger configurations, *J. Heat Transfer* **96,** 265–272 (1974).
4. W. Merzkirch, *Flow Visualization.* Academic Press, New York (1974).
5. H. H. Sogin, Sublimation from disks to air streams flowing normal to their surfaces, *Trans. Am. Soc. mech. Engrs* **80,** 61–71 (1958).
6. A. H. P. Skelland, *Diffusional Mass Transfer.* Wiley, New York (1974).

EFFET DE L'ANGLE D'ATTAQUE SUR LE COEFFICIENT DE TRANSFERT THERMIQUE POUR UNE AILETTE ANNULAIRE

Résumé—Des essais en soufflerie sont menés pour étudier la sensibilité du coefficient de transfert thermique pour une ailette annulaire soumise à des petits angles d'attaque. On distingue trois zones de mesure sur la surface de l'ailette: (I) devant le tube, (II) sur le côté du tube et (III) derrière le tube, avec des mesures séparées sur les deux faces de l'ailette. L'angle d'attaque varie de −2 à 2°. Le coefficient de transfert dans la zone I est fortement sensible à l'angle d'attaque, augmentant d'environ 50 pour cent sur la face pour laquelle la séparation sur le bord d'attaque est activée quand l'angle d'attaque varie. Dans les zones II et III, les accroissements correspondants ne sont que de 10 pour cent. D'autre part, la moyenne sur les deux faces pour chaque zone n'est pas très différente du cas de l'angle d'attaque nul. Par suite la performance globale de l'ailette annulaire n'est pas significativement altérée par un écart de zéro de l'angle d'attaque. Mais puisque les différences entre les coefficients pour les deux faces sont sensibles, une mesure du coefficient sur une seule face conduit à des conclusions erronnées sur la performance globale.

EINFLUSS DES ANSTRÖMWINKELS AUF DEN WÄRMEÜBERGANGSKOEFFIZIENTEN AN RINGFÖRMIGEN RIPPEN

Zusammenfassung—Im Windkanal wurden Messungen zur Untersuchung des Einflusses kleiner Anströmwinkel auf den Wärmeübergangskoeffizienten an einer ringförmigen Rippe durchgeführt. Dazu wurden quasilokale Messungen in 3 Zonen an der Oberfläche der Rippe durchgeführt: (I) an der Vorderseite des Rohres, (II) seitlich am Rohr, (III) an der Rückseite des Rohres, wobei getrennte Messungen an den beiden Seiten der Rippe durchgeführt wurden. Der Anströmwinkel wurde von $-2°$ bis $+2°$ verändert. Der Wärmeübergangskoeffizient in Zone I war stark abhängig vom Anströmwinkel, er erhöhte sich an der Anströmseite um etwa 50 Prozent bei Veränderung des Anblaswinkels von $-2°$ bis $+2°$. Die entsprechenden Erhöhungen in Zone II und III betrugen etwa 10 Prozent. Andererseits zeigte der gemittelte Wärmeübergangskoeffizient beider Seiten für keinen Anströmwinkel im untersuchten Bereich Unterschiede gegenüber dem Anströmwinkel von Null Grad. Aus diesem Grund wird die gesamte übertragene Wärmeleistung bei kleinen Abweichungen des Anströmwinkels von Null Grad nicht signifikant beeinflußt. Da jedoch unterschiedliche Wärmeübergangskoeffizienten an den beiden Seiten nachgewiesen wurden, können Messungen des Wärmeübergangskoeffizienten an nur einer Seite zu fehlerhaften Ergebnissen für die gesamte übertragene Wärmeleistung führen.

ВЛИЯНИЕ УГЛА АТАКИ НА КОЭФФИЦИЕНТ ТЕПЛООБМЕНА КОЛЬЦЕВОГО РЕБРА

Аннотация—Экспериментально исследовалось изменение коэффициента теплообмена кольцевого ребра в аэродинамической трубе при малых углах атаки. Квазилокальные измерения проведены в трех зонах на поверхности ребра: (I) перед трубой, (II) сбоку от трубы и (III) позади трубы; причем особо рассматривались обе плоскости ребра. Угол атаки изменялся от -2 до $2°$. Наиболее чувствителен к величине угла атаки был коэффициент теплообмена в зоне I, увеличиваясь на той или иной плоскости ребра приблизительно на 50% при изменении угла атаки от -2 до $2°$ за счет усиления влияния передней кромки раздела. Соответствующие возрастания в зонах II и III составляли около 10%. С другой стороны, в исследуемом диапазоне при любой величине угла атаки осреднение по двум плоскостям для каждой зоны отличалось незначительно от коэффициента теплообмена при нулевом угле атаки. Поэтому небольшие отклонения значения угла атаки от нуля лишь незначительно влияют на общий коэффициент теплообмена кольцевого ребра. Но вместе с тем, поскольку различие коэффициентов обеих плоскостей незначительно, измерение только на одной плоскости может дать ошибочную величину общего коэффициента.